Decay properties of exotic $N \cong 28$ S and Cl nuclei and the $^{48}Ca/^{46}Ca$ abundance ratio

O. Sorlin, D. Guillemaud-Mueller, A. C. Mueller, V. Borrel, S. Dogny, and F. Pougheon
Institut de Physique Nucléaire, Institut National de Physique Nucléaire et de Physique des Particules (IN2P3), Centre National de la Recherche Scientifique, F-91406 Orsay, France

K.-L. Kratz, H. Gabelmann,* B. Pfeiffer, A. Wöhr, and W. Ziegert†
Institut für Kernchemie, Universität Mainz, D-6500 Mainz, Germany

Yu. E. Penionzhkevich, S. M. Lukyanov, and V. S. Salamatin
Laboratory of Nuclear Reactions, Joint Institute for Nuclear Research (JINR), P.O. Box 79, Dubna, Russia

R. Anne, C. Borcea,‡ L. K. Fifield,§ M. Lewitowicz, and M. G. Saint-Laurent
Grand Accélérateur National d'Ions Lourds (GANIL), BP-5027, F-14021 Caen, France

D. Bazin
Centre d'Etudes Nucléaires Bordeaux, Le Haut Vigneau, F-33170 Gradignan, France

C. Détraz**
Laboratoire de Physique Corpusculaire, Institut des Sciences de la Matière et du Rayonnement (ISMRa), F-14032 Caen, France

F.-K. Thielemann
Harvard-Smithsonian Center for Astrophysics, Cambridge, Massachusetts 02138

W. Hillebrandt
Max Planck Institut für Astrophysik, D-8046 Garching, Germany

(Received 11 November 1992)

Beta-decay half-lives and β-delayed neutron-emission probabilities of the very neutron-rich nuclei ^{44}S and $^{45-47}Cl$ have been measured. These isotopes, which lie at or close to the $N=28$ magic shell, were produced in interactions of a 60 MeV/u ^{48}Ca beam from GANIL (Grand Accélérateur National d'Ions Lourds) with a ^{64}Ni target, and were separated by the doubly achromatic spectrometer LISE (Ligne d'Ions Super Epluchés). Their decay was studied by a β-n time correlation measurement. The results are compared to recent model predictions and indicate a rapid weakening of the $N=28$ shell effect below $^{48}_{20}Ca_{28}$. The nuclear structure effects reflected in the decay properties of the exotic S and Cl isotopes may be the clue for the astrophysical understanding of the unusual $^{48}Ca/^{46}Ca$ abundance ratio measured in the solar system as well as the Ca-Ti-Cr anomalies observed in E. King inclusions of the Allende meteorite.

PACS number(s): 23.40.Hc, 27.40.+z, 21.10.Tg

I. INTRODUCTION

The influence of shell effects has always been a fascinating aspect of the study of very unstable nuclei. The heaviest nuclei, for example, only owe their existence to shell effects [1]. Another interesting question in nuclear structure physics is the persistence of the magicity of closed neutron and/or proton shells for nuclei of very far-off stability. Although experiments are very difficult because of the extremely low production cross sections, there is now hope to reach the doubly magic nucleus ^{78}Ni [2,3] by heavy-ion projectile fragmentation of ^{86}Kr and, similarly, ^{100}Sn by means of a ^{124}Xe beam. For the neutron-magic number $N=20$, a new region of deformation was found in the very neutron-rich Na and Mg nuclei [4]. The properties of these isotopes are still very actively investigated, both experimentally and theoretically [5]. Recent studies with the variational shell model, which reproduces well the properties of the $N=20$ isotones [6], may potentially be pursued also for $N=28$. Far-off stability, i.e., for the elements lighter than Ar, the experimental situation for the $N=28$ isotones is a completely unexplored territory.

This paper reports on a first study of β-decay proper-

*Present address: KSM Analytik GmbH, Wilhem-Maybach Str. 19, 6500 Mainz 42, Germany.
†Present address: CAP DEBIS GEI, Elisabethenstr. 35, 6100 Darmstadt, Germany.
‡Permanent address: Institute of Atomic Physics, P.O. Box M66, Bucharest, Romania.
§Permanent address: Australian National University, G. P. O. Box 4, Canberra ACT 2601, Australia.
**Present address: IN2P3, 20 rue Berbier du Mets, 75640 Paris Cedex, France.

 ©1993 The American Physical Society

ties for Cl and Si isotopes in this region. This work was motivated in part by the fact that these isotopes may play a crucial role as progenitors in astrophysical scenarios leading to the nucleosynthesis of the heavy Ca-Ti-Cr isotopes [7]. By means of intermediate-energy heavy-ion fragmentation it has now become possible to produce and separate these isotopes [8]. Although the production yields are very small, often in the order of only a few events per minute, measurements of half-lives and β-delayed neutron probabilities are feasible: Far-off stability, the β-decay energy (Q_β) becomes sufficiently high to populate unbound states in the daughter nucleus. The observation of the correlated delay neutron emission with a β-particle results in a strong suppression of background.

The paper is organized in the following way. The description of the experimental method, presentation of the data analysis, and comparison of the data to nuclear model predictions are presented first. Finally, we shall show the relevance of this new information to the nucleosynthesis origin of the solar ^{46,48}Ca abundances and the correlated Ca-Ti-Cr isotropic anomalies in certain meteoritic inclusions.

II. EXPERIMENTAL METHOD

A. Production and selection of ^{44}S, $^{45-47}$Cl

The nuclei were produced by fragmentation of a ^{48}Ca beam [9] impinging at 60 MeV/u onto a ^{64}Ni target (116 mg/cm^2). Both beam and target are neutron rich and were chosen in order to maximize the production of neutron-rich isotopes. The selection of the desired nuclei among all fragments was first provided by a magnetic analysis (in Av/Q) of the doubly achromatic spectrometer LISE (Fig. 1) [10]. In addition, a thick degrader (180 mg/cm^2 of aluminum) was used to perform an additional energy-loss selection (approximately in A^3/Z^2) in order to reduce the number of contaminant nuclei. They were deflected by the second magnet according to their different energy loss in the degrader and then suppressed by means of a 18-mm collimator located at the LISE second focal plane. Three settings of the magnetic rigidity ($B\rho$) of the LISE spectrometer were carefully set to optimize the production of ^{44}S, ^{45}Cl, and ^{47}Cl; they are presented in Table I. The result of the on-line selection in the case of ^{47}Cl production is shown in Fig. 2(a) for the selection without the aluminum degrader and for the selection with the degrader in Fig. 2(b).

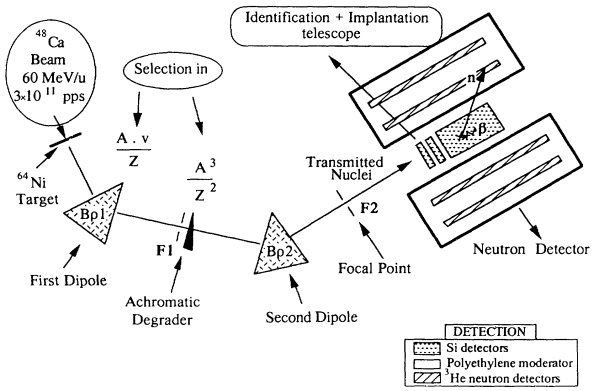

FIG. 1. Schematic representation of the LISE spectrometer and the detection system.

The collection rate for these nuclei is very sensitive to the magnetic rigidity of the first dipole. The outgoing fragments exhibit a narrow energy distribution principally due to the fragmentation process in the relatively thin production target. Thus, a variation of only 3% in the magnetic rigidity $(B\rho)_1$ of the first dipole eliminates 90% of the transmitted nuclei.

B. Identification

The selected nuclei were detected in a telescope composed of three detectors. The first two are implanted passivated silicon detectors of 300-μm thickness whereas the third is a Si(Li) detector of 5500-μm thickness. The

TABLE I. Number of implanted and selected nuclei and detected β-n coincidences for three different magnetic rigidities.

$B\rho$ settings [$T\,m$] $((B\rho)_1,(B\rho)_2)$	Implanted nuclei (counts)	Nuclei selected in the ΔE-TOF window (counts)	Number of β-n coincidences
(2.85,2.641)	^{44}S (18724)	^{44}S (18724)	575
	^{46}Cl (1515)	^{46}Cl (1515)	131
	^{42}P (491)	^{42}P (464)	14
	^{43}S (164)		
(2.886,2.56)	^{45}Cl (20083)	^{45}Cl (20083)	880
	^{46}Cl (3520)	^{46}Cl (1596)	147
	^{44}S (3256)		
	^{43}S (456)		
(2.95,2.619)	^{47}Cl (9724)	^{47}Cl (9690)	24
	^{49}Ar (8237)		
	^{49}S (693)		

identification was determined on-line by comparison of energy-loss signals produced in the first Si detector to energy-calibrated signals from a pulser. The pulser was adjusted to correspond to the expected energy loss of each nucleus according to tabulated values [11]. The identification is fully described below in the case of the ^{47}Cl setting.

A momentum acceptance of $\pm 1.4\%$ was chosen to favor a high transmission rate; this, however, led to a large energy distribution for a given nucleus. Hence, Fig. 2(b) shows that ^{45}S, ^{47}Cl, and ^{49}Ar have very similar values of time of flight and energy loss. Off-line, a more refined analysis using a redundant identification combining energy losses ($\Delta E1$, $\Delta E2$), total energy (E), time of flight τ_{TOF}, and focal plane position has confirmed the identification of the nuclei. Figure 3(a) represents a calculated two-dimensional display ($\Delta E1$, τ_{TOF}) in the case of ^{47}Cl production with the degrader. The expected energy loss of ^{47}Cl deduced from Fig. 2(b) is also represented in this figure between the two horizontal lines. It shows that, even if ^{47}Cl is well centered, six nuclei lie almost in this energy-loss range.

For each dipole, the velocity β of the nuclei is given by the relation

$$B\rho = 3.105 A\beta\gamma / Q \ . \tag{1}$$

The time of flight τ_{TOF} is calculated as the sum of the times in the first section (length L_1, magnetic field B_1) and in the second one (L_2, B_2) of the spectrometer:

$$\tau_{\mathrm{TOF}} = \frac{L_1}{\beta_1} + \frac{L_2}{\beta_2} \ , \tag{2}$$

with $\beta_1/\beta_2 = B_1/B_2$, and $L_1 = 758.5$ cm and $L_2 = 1038.6$ cm. The experimental time of flight is not an absolute one because it was measured with the radio-frequency pulses of the primary beam delivered by the cyclotron. Then, only the difference $\Delta\tau_{\mathrm{TOF}}$ between each nucleus is relevant. According to Fig. 2(b), this value should be ≈ 3 ns. This is moreover consistent with the calculated τ_{TOF} difference between ^{45}S and ^{47}Cl [Fig. 3(a)]. Finally, a position determination (in units of mm) [$P(A,Z)=0$ for a selected nucleus] of the fragments after the second dipole:

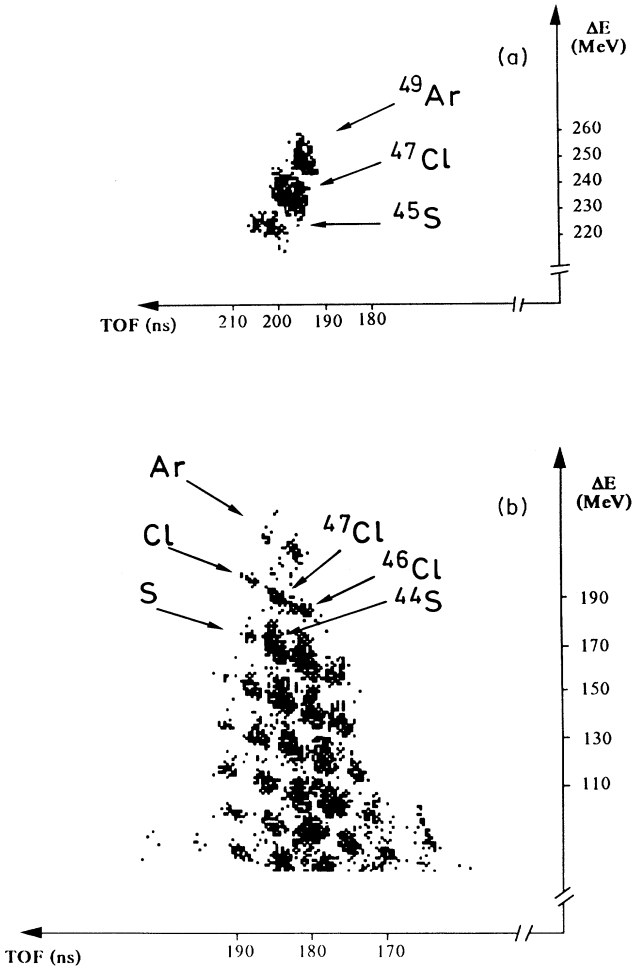

FIG. 2. (a) ΔE (energy loss) vs TOF (time of flight) on-line matrix for the first magnetic setting without any degrader. (b) (ΔE, TOF) on-line matrix optimized for the ^{47}Cl transmission with an Al (180 mg/cm^2) intermediate degrader.

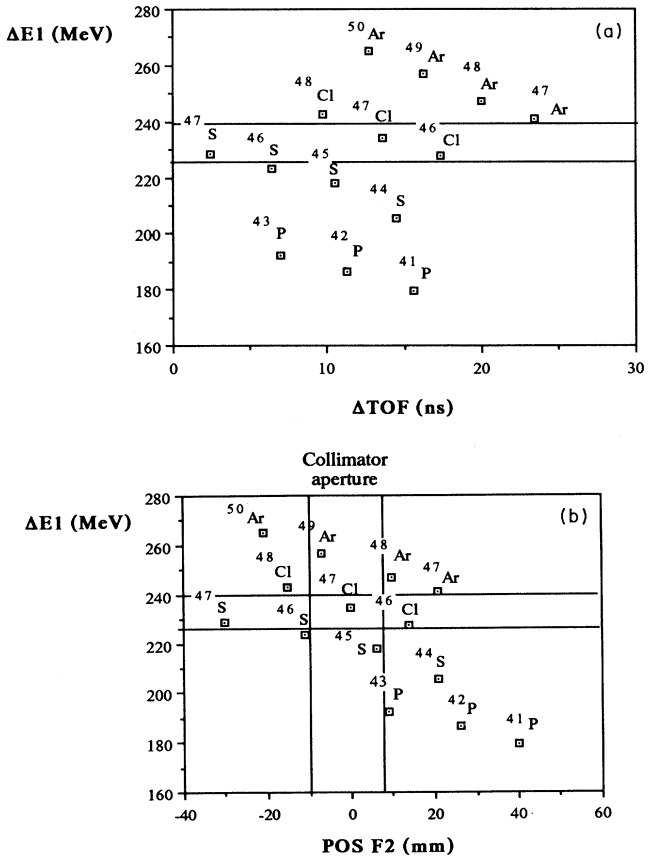

FIG. 3. (a) Two-dimensional representation ($\Delta E1, \Delta\tau_{\mathrm{TOF}}$) calculated for the conditions of the present experiment. The selected zone on the y axis corresponds to the range of energy loss of ^{47}Cl due to the chosen momentum acceptance of the spectrometer. (b) Position dependence at the focal plane $F2$ versus energy loss $\Delta E1$ for different isotopes.

$$P(A,Z)=100\frac{E_f^3(A,Z)-E_f^2(A,Z)}{E_f^2(A,Z)}\frac{D_{\mathrm{LISE}}}{2}, \quad (3)$$

where E_f^3 is the energy at the output of the degrader for a given fragment, E_f^2 is the energy preferentially transmitted by the second dipole, and D_{LISE} [mm/%] is the momentum dispersion of the second dipole, shows that only the nuclei ^{49}Ar, ^{47}Cl, and ^{45}S could be transmitted through the collimator [Fig. 3(b)]. This confirms without any doubt the identification of ^{47}Cl.

C. Data acquisition

Each isotope under study was, as previously described, identified on-line by a combined measurement of its time of flight through the spectrometer and its energy loss in the first 300-μm silicon detector. Two single-channel analyzers examined the ΔE and τ_{TOF} pulse heights. Each time a detected nucleus lay within the selected ΔE-τ_{TOF} window thresholds, the beam was stopped. The cutoff duration lasted about five times the expected β half-life of the implanted nucleus. During this time, a second data acquisition recorded coincidences between a β particle and a neutron at low background. A set of plastic scintillators above and below the neutron counter was used to detect cosmic muons which could induce neutron background. Thus, in the subsequent off-line analysis it was possible to discriminate β-muon coincidences from true β-neutron events. With this setup, almost all β-delayed neutron coincidences could be directly correlated to implanted precursor nuclei. This triple coincidence (nucleus-β-neutron) leads to a very low background rate. The small remaining background contribution comes from the decay of the contaminants implanted slightly prior to a desired nucleus. The evaluation of this contamination rate is explained in the following chapter.

III. DATA ANALYSIS

A. Background evaluation

Each nucleus transmitted by the spectrometer and implanted in the third silicon detector, may give rise to a β-n decay (whose half-life is often unknown). If this nucleus is not selected in the ΔE-TOF window, it will not trigger the second acquisition used for radioactivity measurements and will not stop the beam. This type of event represents the principal source of background. In this case, the decay event could be fortuitously correlated with that of a nucleus implanted later. Hence, it is important to carefully choose the ΔE-TOF window. This window can either (i) select all the transmitted nuclei or (ii) only the desired one. With the first solution, one considerably reduces the background because the acquisition is triggered for each transmitted nucleus and the beam is cut off at each time. The only contamination then will be due to nuclei implanted between the detection of a nucleus and the beam cutoff. The drawback of this method is to lose beam time in an amount which depends on their production rates and on their half-lives (the longer the half-life, the longer one must wait for the radioactive decay). With the second method, one just takes the time necessary to measure the desired nucleus' decay, but sometimes one needs to deal with unknown contaminants implanted prior to the beam cutoff. Simulations of the experimental time sequences of implanted nuclei and beam cutoff have been made to estimate the contribution of the background. An example of this estimation is shown in Fig. 4.

B. Efficiency calibrations

The transmitted nuclei were implanted into the third detector which also served for the β detection (see Fig. 1). The telescope was surrounded by a nearly 4π neutron counter, composed of two concentric rings consisting of 39 ^{3}He-proportional counters embedded in a polyethylene moderator matrix. The detector has a nearly energy-independent efficiency of $\varepsilon_n=27\pm2\%$ up to $E_n\approx2$ MeV and has no low-energy cutoff, as scintillators do. The β detection efficiency ε_β is deduced from the following relation:

$$\varepsilon_\beta=\frac{N_{\beta n}}{N_{\mathrm{nuclei}}P_n} \quad (4)$$

with $N_{\beta n}$ being the number of β-neutron coincidences, N_{nuclei} the number of nuclei detected, and P_n the delayed-neutron emission probability. This detection system was calibrated with the well-known values of $T_{1/2}=10.3\pm0.2$ ms and $P_n=100\%$ of ^{15}B [12,13], which led to $\varepsilon_\beta=60\pm5\%$.

C. $T_{1/2}$ and P_n results

The number of implanted and selected nuclei is given in Table I together with the number of β-n coincidences for each $B\rho$ setting. The half-lives were deduced from constructing a time histogram of the β-n ($N_{\beta n}$) coincidences detected after the identification of the corresponding nucleus. The decay curves were compared with those obtained with the simulation mentioned in Sec. III A. This showed that, except for one set of measurements (^{45}Cl) for which a contaminant with a short half-life was implanted (Fig. 4), a linear subtraction of the background was sufficient. To perform a better determination of the ^{45}Cl half-life, the first 240 ms were skipped in order to avoid the steeper slope due to the ^{44}S, ^{46}Cl contaminations (see their contamination rate in Table I). The decay curve was then fitted keeping the background fixed.

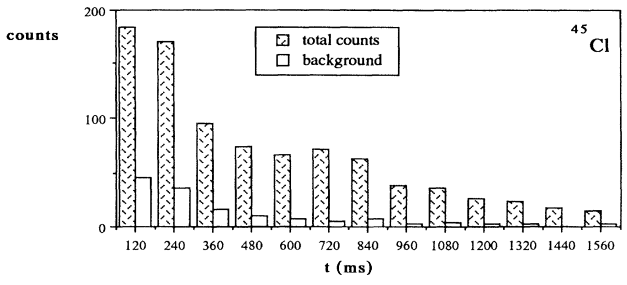

FIG. 4. Estimation of the importance of the β-n background compared with the β-n events from ^{45}Cl decay.

TABLE II. Comparison of half-lives deduced from different fitting procedures.

Nucleus	$T_{1/2}$ (ms) MINUIT[a]	$T_{1/2}$ (ms) MINUIT[b]	$T_{1/2}$ (ms) FITB01[c]	$T_{1/2}$ (ms) Mean value
^{44}S	125±9	122±13	121±9	123±10
^{45}Cl	400±45	395±48	405±35	400±43
^{46}Cl	237±31	230±29	202±50	223±37

[a]Maximum likelihood minimization with the MINUIT [14] code.
[b]χ^2 minimization with the MINUIT code.
[c]χ^2 minimization with FITB01 [15] code.

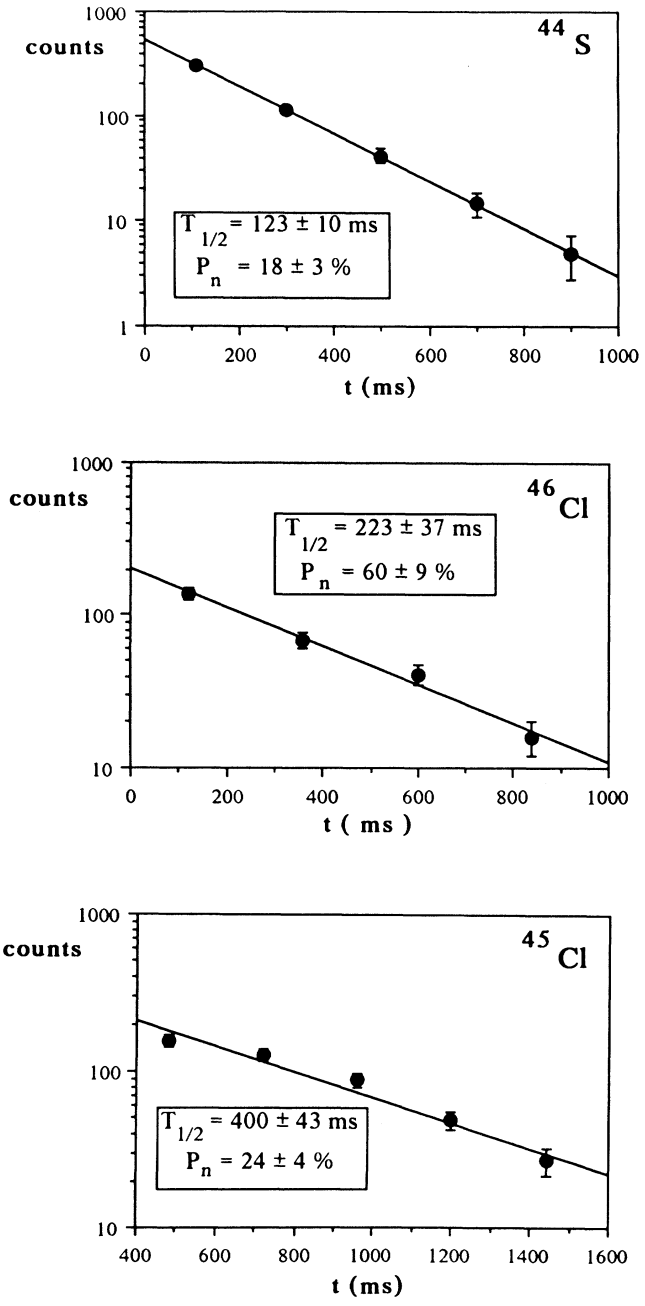

FIG. 5. Experimental decay curves for ^{44}S, ^{45,46}Cl. Their half-lives ($T_{1/2}$) and β-delayed neutron emission probabilities (P_n) are also given.

For the other two isotopes, considering a linear subtraction only, a single decay component was observed (see Fig. 5). The three first results have been obtained with two different fit algorithms MINUIT and FITB01 with χ^2 or maximum likelihood minimization. The half-lives are presented with their standard deviation. These results given in Table II are consistent.

The somewhat longer half-life of ^{44}S (200^{+50}_{-30} ms) found in Ref. [16] may be explained by two reasons: (i) an underestimation of the background (this experiment did not use an energy degrader, which led to a higher contamination rate due to all the nuclei implanted) and (ii) the time window for recording the decay events, fixed for a whole set of nuclei, was too short in this case (about three times the half-life). The slope of the decay curve was then difficult to determine without ambiguity.

In the case of ^{47}Cl, with 9724 nuclei implanted (Table III), we observed only very few β-n coincidences, compatible with $P_n \leq 3\%$. Therefore, no reliable half-life could be deduced. The P_n values were determined by the ratio of true β-n coincidences and the number of implanted nuclei corrected by the β-n detection efficiency:

$$P_n = \frac{N_{\beta n}}{N_{\text{nuclei}} \varepsilon_\beta \varepsilon_n} . \quad (5)$$

IV. COMPARISON WITH MODEL PREDICTIONS

When comparing our experimental data to the TDA model predictions of [17], one observes only moderate agreement: the $T_{1/2}$ of ^{44}S and ^{45}Cl—both representing "key nuclei" for the nucleosynthesis of ^{46}Ca (see Sec. V)—were found to be experimentally shorter by factors of 3 and 4, respectively. However, even more recent and

TABLE III. Numbers of nuclei and contaminants as well as P_n results for the three settings of LISE, with $\varepsilon_\beta = 0.6$ and $\varepsilon_n = 0.27$.

Analyzed nucleus	Implanted nuclei N_{nuclei}	Total $N_{\beta n}$ detected (without background subtraction)	P_n (%)
^{44}S	18724	575 (background ≈45)	18±3
^{45}Cl	20083	880 (background ≈140)	24±4
^{46}Cl	3111	285 (background ≈6)	60±9
^{47}Cl	9724	24 (background ≈17)	<3

sophisticated QRPA models [18–20] seem to have difficulty in this mass region due to the rapid, and partly unexpected, nuclear-shape changes in the neutron-rich vicinity of the doubly-magic nucleus $^{48}_{20}Ca_{28}$ (for a recent review, see for example, [5]).

All recent (macroscopic-) microscopic mass models, e.g., the finite-range liquid-drop (FRLD) model [21], the finite-range droplet (FRD) model [22] in its present form [23], as well as the extended Thomas-Fermi with Strutinski-integral (ETFSI) model [24], agree in that the neutron-rich isotopes of $_{16}$S to $_{18}$Ar have a rather "soft" potential-energy surface with several shallow minima for different shapes (i.e., different deformations). These minima are often separated by "barriers" of only a few hundred keV height. In the three models above, per definition, the lowest calculated minimum represents the ground-state shape of the nucleus. Hence, it is not surprising that occasionally quite different ground-state deformations are listed in the mass tables for the same isotope (see Table IV). Since nuclear (quadrupole) deformation is an important input parameter for the quasirandom phase approximation (QRPA) calculations of Gamow-Teller strength function S_{GT}, which determines the ground-state spin and parity and the wave functions of the β-decay mother and daughter nuclei, a "wrong" deformation often leads to a "wrong" GT-decay pattern finally resulting in a "wrong" half-life ($T_{1/2} \propto 1/S_{GT}$) and/or a "wrong" P_n value (see, for example, [25]).

Another problem in the calculation of β-decay properties within the present QRPA models is in their model-inherent assumption of equal ground-state deformation for both mother and daughter nuclei. As can be seen from Table IV, in the $N \approx 28$ $_{16}$S to $_{18}$Ar region, this may not always be the case. Therefore parent-daughter pairs with different deformations or shape coexistence cannot be treated properly in the current shell models. In consequence, again "wrong" S_{GT} and "wrong" $T_{1/2}$ and P_n values may result. Hence, reliable predictions of unknown β-decay features in the mass region below ^{48}Ca cannot be made in a straightforward way. In this paper we use the most recent QRPA model of Möller and Randrup [19] with a simple residual GT interaction. The Nilsson model is applied for determining the wave functions of initial and final nuclei. The shell-dependent **L·S**- and L^2-strength parameters of the modified oscillator potential recommended by Ragnarsson and Sheline [27], with slightly changed values for the $N=3$ oscillator shell [28], were used. Instead of the earlier used BCS code [18], the more sophisticated Lipkin-Nogami approximation [29] has been applied to calculate pairing correlations. Quadrupole deformation parameters (ε_2) and β-decay energies Q_β were taken from the above mass models. In the following we will briefly discuss the $T_{1/2}$ and P_n calculations against our experimental findings.

As can be seen from Table IV, the neutron magic ($N=28$) isotope $^{44}_{16}$S is predicted to be either spherical or oblate, whereas its daughter ^{44}Cl is assumed to have a prolate g.s. deformation. However, in the light of the above discussion of the potential-energy surface in this mass region and the possible shape changes in the vicinity of the $N=28$ shell, none of the predicted g.s. deformations can be excluded *a priori*. Since no detailed spectroscopic information of ^{44}S β decay (or its close neighbors) is available, one can only hope that the integral quantities $T_{1/2}$ and P_n may to some extent reflect nuclear structure. In Fig. 6, theoretical GT strength functions are shown for three "typical" shapes, prolate with $\varepsilon_2=0.125$, spherical and oblate with $\varepsilon_2=-0.25$. As the influence of Q_β is negligible in this case, the differences in $T_{1/2}$ and P_n must be due to the different nuclear structures reflected in the S_{GT} pattern. From this figure it is evident, that a "short" $T_{1/2}$ together with a "small" P_n as observed in the experiment can only be obtained when assuming that the g.s. of the semimagic nucleus ^{44}S is not spherical but *oblate* deformed.

TABLE IV. Predictions of deformation parameters ε_2 and β-decay energies Q_β from the recent FRLDM [21], FRDM [23], and ETFSI [24] mass models. The Q_β of the last column [26] are either experimental or deduced from extrapolations (recognized by the sign *) from the mass surfaces.

	ε_2			Q_β (MeV)			
	FRLDM	FRDM	ETFSI	FRLDM	FRDM	ETFSI	Expt. or Extrap.*
Isotope	[21]	[23]	[24]	[21]	[23]	[24]	[26]
$^{43}_{16}S_{27}$	0.14	0.18	0.17	12.67	12.04	12.61	11.55±0.86
$^{44}S_{28}$	−0.14	0	−0.23	11.49	10.66	11.91	10.10*
$^{45}S_{29}$	−0.17	0.16	−0.18	14.62	15.10	15.34	14.72*
$^{46}S_{30}$	0.19	0.20	−0.22	15.19	14.83	15.56	13.00*
$^{44}_{17}Cl_{27}$	0.12	0.14	0.16	13.20	12.89	11.58	12.27±0.22
$^{45}Cl_{28}$	−0.15	−0.16	−0.20	11.63	13.07	11.13	10.80±0.65
$^{46}Cl_{29}$	−0.18	−0.18	−0.18	15.96	16.19	14.17	15.46*
$^{47}Cl_{30}$	0.19	−0.20	−0.22	16.26	14.70	15.01	15.34*
$^{45}_{18}Ar_{27}$	0.10	−0.18	0.14	8.55	7.13	7.82	6.89±0.06
$^{46}Ar_{28}$	0.03	0	−0.20	6.97	6.81	7.38	5.70±0.04
$^{47}Ar_{29}$	−0.11	−0.18	−0.22	10.66	11.98	10.79	9.79±0.10
$^{48}Ar_{30}$	−0.19	−0.20	−0.22	10.83	10.63	11.12	9.55*

A similarly unclear situation exists for the β decay of $N=28$ isotone ^{45}Cl (see Table IV). Whereas all three mass models predict oblate deformations for the parent nucleus, the daughter ^{45}Ar is assumed to be either prolate or oblate deformed, but not spherical. With its known g.s. spin of $J^{\pi}=7/2^{-}$, however, ^{45}Ar presumably has a prolate shape. Using the Q_{β} value of the FRLD or ETFSI models and taking prolate deformation for the ^{45}Cl–^{45}Ar pair, we calculate $T_{1/2} \cong 460$ ms and $P_n \cong 44\%$, in fair agreement with observations. When assuming the more unlikely spherical or oblate shapes, shorter $T_{1/2} \cong 250$–260 ms are obtained. From these results we can again speculate that the neutron-magic nucleus is not spherical.

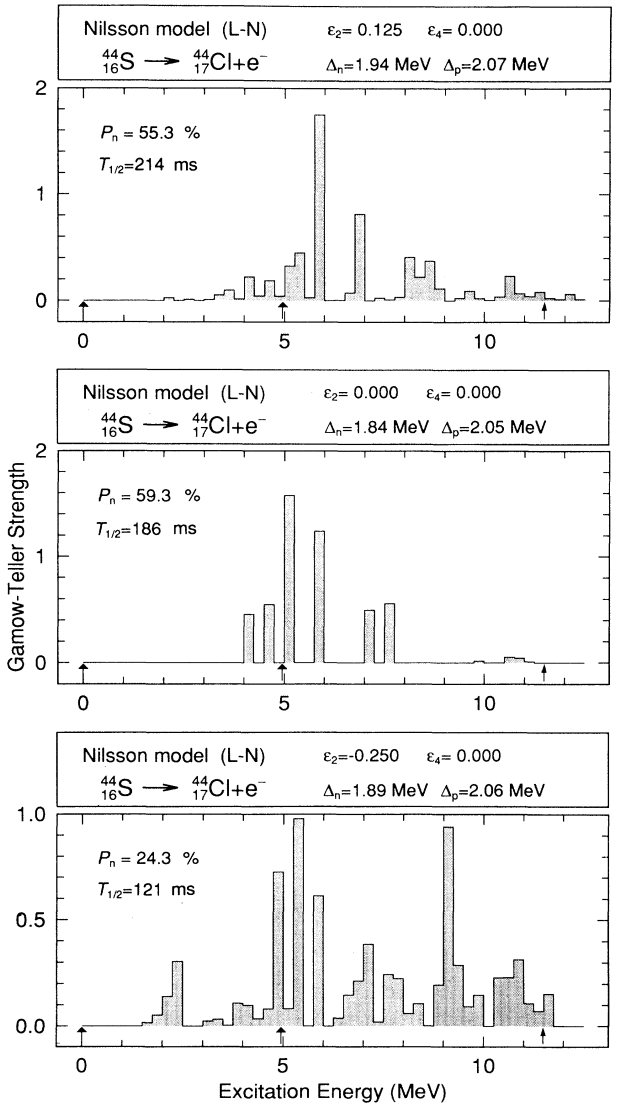

FIG. 6. Theoretical Gamow-Teller strength functions for $^{44}_{16}$S decay are shown for different ε_2 nuclear shape assumptions (from the upper curve down to the lower: prolate, spherical, oblate). The arrows on the horizontal axis show the position of the predicted B_n ($\cong 5$ MeV) and Q_{β} ($\cong 11.5$ MeV) values, see text for comments.

For β decay of ^{46}Cl, a "short" $T_{1/2}$ together with a "small" P_n, as observed in experiment, can only be obtained when assuming oblate deformation. A (near-) spherical shape, as might be inferred from the FRLD and FRD model predictions for the ^{46}Ar daughter, would lead to $T_{1/2} \cong 1$ s and $P_n \cong 90\%$. In the case of ^{47}Cl β decay, all three models consistently predict an oblate deformation for both parent and daughter. With $Q_{\beta} \cong 14.7$ MeV (FRDM) and $\varepsilon_2 \cong 0.21$, one calculates $T_{1/2} \cong 95$ ms and $P_n \cong 100\%$; when using the higher β-decay energy of FRLDM, the $T_{1/2}$ drops to about 40 ms with still a large $P_n \cong 70\%$. Unfortunately, so far no experimental value for the half-life is available, and only evidence for a "very small" P_n value—in contrast to *all* present model predictions—has been obtained. A possible explanation may lie in low-lying first-forbidden (ff) β transitions "missing" in the QRPA models which only describe GT decay. For oblate deformation of ^{47}Cl, the lowest-energy GT branch is predicted close to $B_n \cong 4$ MeV in ^{47}Ar, thus explaining the large theoretical P_n value. With the $[211]\frac{3}{2}^{+}$ g.s. configuration of $\pi d_{3/2}$ parentage for $^{47}_{17}$Cl, and the $[312]\frac{3}{2}^{-}$ g.s. configuration of $\nu p_{3/2}$ shell-model origin, a strong ff g.s. transition is possible. When assuming, for example, a logft $\cong 6.0$, a considerable part of the sum-rule β strength would then lie below B_n, resulting in a "small" P_n value—without influencing in the theoretical $T_{1/2}$ too much.

Summarizing, we can conclude that—due to the specific nuclear structure—straightforward predictions of β-decay properties in the $_{16}$S to $_{18}$Ar region are not possible. As we have seen, big surprises are possible even for semimagic isotopes which, from simple considerations, may be expected to be (near) spherical. However, the fact that our experimental results on $T_{1/2}$ and P_n of $^{44}S_{28}$ and $^{45}Cl_{28}$ indicate collectivity, provides first evidence for a rapidly vanishing $N=28$ shell strength "below" $^{48}_{20}Ca_{28}$. This observation is in agreement with the recent mass-model predictions. In order to obtain better insight into the phenomenon of shape changes, detailed spectroscopic studies as well as fully microscopic shell-model calculations are requested. Finally, as a consequence of our findings, present predictions of β-decay properties of neutron-rich Ar isotopes—of importance as possible astrophysical progenitors of ^{48}Ca (see Sec. V)—should not be taken too seriously. From what we have seen for the $N \cong 28$ sulfur and chlorine isotopes, it is necessary to *measure* at least $T_{1/2}$ and P_n values of neutron-rich Ar isotopes, if not their detailed level schemes. Such experiments are foreseen at GANIL using the LISE3 spectrometer [30].

V. CORRELATED Ca-Ti-Cr-Fe-Ni ANOMALIES IN METEORITES

A. Nucleosynthesis origin and astrophysical sites

The two existing scenarios to produce correlated Ca-Ti-Cr anomalies in meteoritic inclusions [a rapid neutron-capture process and a neutron-rich nuclear

statistic equilibrium (NSE) model] are discussed in the light of present experimental findings. They indicate in a first estimate a change to required neutron densities of $n \cong 3 \times 10^{19}$ cm^{-3} and time scales of 1 s for the first scenario, which are typical for explosive Si-burning zones in type-II supernovae, adjacent to zones which experience *r*-process conditions. These are conditions close to a very neutron-rich NSE, which makes a merging of both scenarios possible. Such conclusions have to be verified in future calculations which will have to include further knowledge of the properties of neutron-rich Cl and Ar isotopes and a proper treatment of an alpha-rich (see Sec. V E) rather than a normal freeze-out of charged-particle reactions. The closeness of the *r*-process site ensures a correlation of the Ca-Ti-Cr anomalies with *r*-process anomalies in meteorites.

B. Situation before the present experiment

Correlated anomalies of ^{48}Ca, ^{50}Ti, ^{54}Cr, ^{58}Fe, ^{64}Ni, ^{66}Zn, and also *r*-process isotopes in CaAl-rich inclusions have been found by a number of investigators [31–40]. Early theoretical attempts to explain these anomalies included three possible approaches: (1) neutron-rich nuclear statistical equilibria (NSE [41]), (2) neutron-capture processes ($n\beta$ process [42]), and (3) proton-rich environments (the *rp* process [43]), which were mainly parameter studies and not linked to astrophysical models. These were later refined by Hartmann *et al.* [44] who used a superposition of NSE zones with varying neutron excess—the multizone mixing (MZM) model—and by Ziegert *et al.* [45] and Hillebrandt *et al.* [46]. They introduced into the neutron-capture process (also called βn_d process) improved β-decay properties, in particular effects of β-delayed neutron branching around ^{48}Ca. Lee [47] could show that, when utilizing the predictions for all isotopes, the *rp* process and the plain $n\beta$ process could be excluded from explaining the Ca-Ti anomalies. The MZM model and the βn_d process did not cause such contradictions.

Sandler *et al.* [42] had to postulate nonstatistical neutron-capture cross sections for the reaction ^{46}K(n,γ) and ^{49}Ca(n,γ) in a neutron-capture process, caused by hypothetical low-lying *s*-wave resonances. In the latter case, indeed, such a resonance was observed experimentally in the inverse process, i.e., neutron emission following the β decay of ^{50}K [48]. However, subsequent measurements of the partial decay widths of this state [45] excluded the explanation of the meteoritic ^{49,50}Ti abundances suggested by Sandler *et al.* [42]. In a different approach, Hartmann *et al.* [44] in their neutron-rich NSE model were able to produce Ca-Ti anomalies by utilizing a mixed-zone approach with varying neutron excess for a normal freeze-out from nuclear statistical equilibrium at 3×10^9 K, as it was expected from the innermost zones of type-II supernova ejecta (or possibly even in the central mass zones of type-Ia supernovae). The observed ratio of ^{48}Ca/^{50}Ti=3.55 could not be explained; they obtained only a ^{48}Ca/^{50}Ti ratio of 0.8. The predicted ^{66}Zn enhancements were much larger than later observed. These discrepancies might, however, be explained by element fractionation due to the differing volatility of different elements (e.g., Zn). On the other hand, β-decay properties of unstable primary nuclei were not taken into account in this approach which have been shown to play an important role in the vicinity of ^{48}Ca [45].

One of the possible sites of neutron-capture scenarios is the He zone of massive stars during a type-II supernova explosion. Blake *et al.* [49] and Cowan *et al.* [50] could show that these zones will not attain *r*-process conditions by (α,n) reactions, as expected initially [51,52], but the neutron densities could be large enough to cause nuclear transmutations and nonsolar neutron-rich patterns. The attempts by Ziegert *et al.* [45] and Hillebrandt *et al.* [46] made also use of β-decay properties of neutron-rich nuclei. Of particular importance was the strong variation in the P_n values (neutron emission after β decay of the parent nucleus) of the neighboring isotopes ^{48}K (1.1%) and ^{49}K (86%). This allowed a large enhancement of the ^{48}Ca abundance and a reduction of ^{49}Ti without the postulated nonstatistical neutron-capture cross sections [42].

The studies of Ziegert *et al.* [45] considered only neutron-capture reactions in each isotopic chain. Beta decay was considered *after* the sequence of neutron captures ended. Hillebrandt *et al.* [46] performed a complete network calculation which included neutron and charged-particle captures as well as photodisintegrations and β decays. With the temperature chosen ($T_9 < 1$), charged-particle captures and photodisintegrations were, however, negligible. Both of these investigations assumed a solar system composition for nuclei heavier than Si. The latter, with strong abundance changes between odd-*Z* and even-*Z* chains, was essential for their results. For a neutron exposure of about 5×10^{-5} mol cm^{-3} s, ^{48}Ca was found to be formed mainly from the even-*Z* $_{18}$Ar-progenitors ^{48}Ar$(\beta^-)^{48}$K$(\beta^-)^{48}$Ca and ^{49}Ar$(\beta^-)^{49}$K$(\beta^- n)^{48}$Ca, whereas the abundance distribution of $_{16}$S isotopes has not yet reached $A = 46$. Thus, a low production of ^{46}Ca originates mainly from the odd-*Z* (low initial abundance) $_{17}$Cl progenitors ^{46,47}Cl.

It should be noted, however, that the results of Hillebrandt *et al.* [46] depended on the—at that time unknown—$T_{1/2}$ and P_n values of neutron-rich S, Cl, and Ar isotopes for which model predictions [53,17] had to be used. The situation in 1986 is summarized in Fig. 7 for a neutron density 5×10^{-5} mol cm^{-3}, but without constraints on the process duration. A strong time limitation of $\tau \cong 50$ ms for the βn_d process was caused by the short $T_{1/2}$ of ^{44}S of about 310 ms [17], as shown in Fig. 8. With this exposure time, one obtains a neutron density of $\rho Y_n \cong 10^{-3}$ mol/cm^3; therefore, the neutron-capture times $T_{1/2}(n)$ given in Fig. 7 would have to be divided by a factor of 20. As the β decay of ^{44}S is preferable over neutron capture [$T_{1/2}(n) \cong 1$ s] under these conditions, the neutron capture on ^{45}Cl essentially "measures" the abundance transfer to ^{46,47}Cl. Thus, short time scales are required (see Fig. 8) to minimize the leakage from ^{44}S into the Cl chain in order to obtain a high final ^{48}Ca/^{46}Ca ratio. In the Cl chain itself, successive neutron captures will also proceed up to ^{46,47}Cl. The most important quantity of these isotopes was found to be their βn_d-branching ratio. As an example, Fig. 9 demonstrates the influence of the P_n(^{47}Cl) on the final ^{48}Ca/^{46}Ca ratio. With a fixed

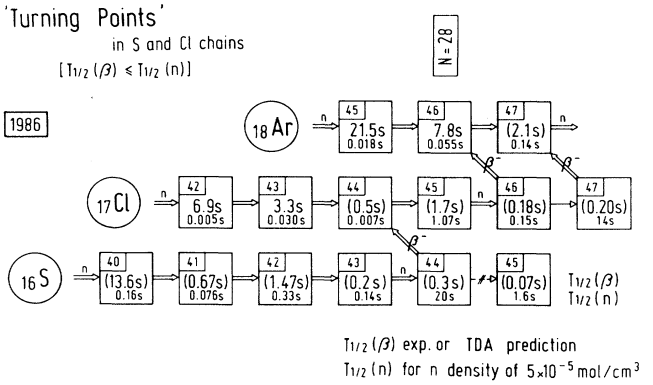

FIG. 7. Neutron capture path in the $_{16}$S to $_{18}$Ar chains [7] for a stellar temperature of $T=8\times10^8$ K and a neutron density of 5×10^{-5} mol cm^{-3}, predicted in 1986.

theoretical $P_n(^{46}\mathrm{Cl})=30\%$, the solar ratio of ^{48}Ca/^{46}Ca [54] can be reproduced with each $P_n(^{47}\mathrm{Cl})$, whereas the exotic abundance ratio observed in the EK-1-4-1 meteoritic inclusion is only reached with a "low" $P_n(^{47}\mathrm{Cl})$. In fact, the effects of the β-decay properties of ^{44}S and ^{46,47}Cl on the resulting ^{48}Ca/^{46}Ca ratio are interrelated, and it was strongly requested [46] to measure these important nuclear physics quantities in order to restrict the astrophysical parameter space.

C. Astrophysical environment

One has to see these results in an astrophysical context and inquire whether they leave room for a meaningful scenario. Recently Harper *et al.* [40] showed that the ^{96}Zr anomaly and the Ca-Ti anomalies are correlated and found in the same inclusions. That indicates that the *r*

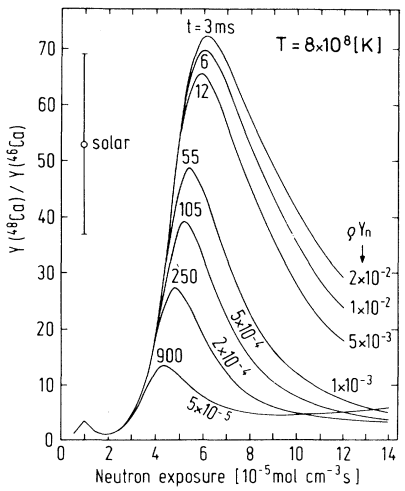

FIG. 8. Abundance ratio ^{48}Ca/^{46}Ca as a function of neutron exposure for various combinations of neutron densities ($Y_n\rho$) and exposure times in milliseconds. Given is the exposure time at which the maximum abundance ratio was obtained. Beta-decay half-lives from Klapdor *et al.* [17] have been used.

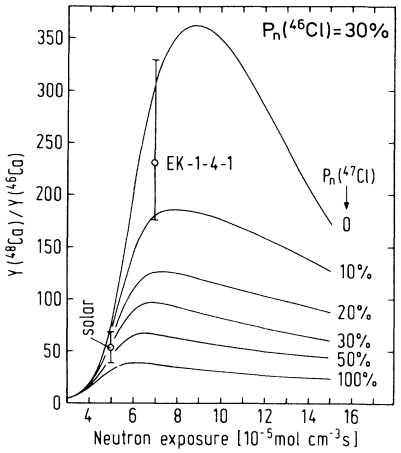

FIG. 9. Abundance ratio ^{48}Ca/^{46}Ca as a function of neutron exposure for various assumptions on $P_n(^{47}\mathrm{Cl})$. For discussion, see text.

process and the Ca-Ti anomalies come from the same event, which can only be a type-II supernova. Both scenarios, neutron-rich Si-burning resulting in an NSE [44] and explosive He burning, as suggested by Ziegert *et al.* [45] and Hillebrandt *et al.* [46] will have time scales of the order of 1 s, but in no case 50 ms. Therefore, the result before the present experiments discussed in Sec. V B should be considered as a mathematical solution but not necessarily as an astrophysically meaningful one. Another problem for explosive He burning is the requirement on the neutron source.

Both papers by Ziegert *et al.* [45] and Hillebrandt *et al.* [46] assumed temperatures of $T_9<1$, a necessary condition if photodisintegrations should be negligible. Under such conditions only (α,n)-neutron sources like ^{13}C, ^{18}O, or ^{22}Ne can provide strong neutron fluxes. We can then estimate the change in neutron abundance by the following equation:

$$\frac{d(Y_n)}{dt}=\rho N_A\langle\sigma v\rangle_{(\alpha,n)}Y_\alpha Y_{\mathrm{ns}} - \rho N_A\langle\sigma v\rangle_{(n,\gamma)}Y_n f Y_{56}\ , \tag{6}$$

where abundances Y are related to number density n by $Y=n/(\rho N_A)$. Here the first term gives a positive contribution from the neutron source Y_{ns} (standing for ^{13}C, ^{18}O, or ^{22}Ne) and the second negative term describes the neutron poisons. With ^{56}Fe having a dominant abundance and neutron-capture cross section, we parametrize all neutron poisons by the Fe cross section and abundance. The factor f corrects for all other neutron poisons. An equilibrium between neutron captures and neutron-producing reactions will be attained after a short time scale, dictated by fast neutron-capture reactions and resulting in $d(Y_n)/dt=0$. This leads from Eq. (6) to

$$\rho Y_n=\frac{\rho N_A\langle\sigma v\rangle_{(\alpha,n)}Y_\alpha Y_{\mathrm{ns}}}{N_A\langle\sigma v\rangle_{(n,\gamma)}f Y_{56}}\ . \tag{7}$$

The time scale for the depletion of the neutron source, i.e., neutron irradiation, is given by

$$\frac{d(Y_{\rm ns})}{dt}=-\frac{1}{\tau}Y_{\rm ns} \quad \text{with } \tau=[N_A\langle\sigma v\rangle_{(\alpha,n)}\rho Y_\alpha]^{-1} . \quad (8)$$

Combining Eqs. (7) and (8) gives an expression for $(\rho Y_n)\tau$

$$\rho Y_n\tau=\frac{1}{N_A\langle\sigma v\rangle_{(n,\gamma)}}\frac{Y_{\rm ns}}{fY_{56}}$$
$$=2.6\,Y_{\rm ns}/f\times10^{-2} . \quad (9)$$

Here we made use of thermonuclear reaction rates for neutron capture on ^{56}Fe by Bao and Käppeler [55] ($N_A\langle\sigma v\rangle_{(n,\gamma)}=1.915\times10^6$) and a solar system abundance of $Y_{56}=2\times10^{-5}$ [56]. With $(\rho Y_n)\tau\cong5\times10^{-5}$, we obtain the necessary condition, $Y_{\rm ns}\cong f(1.92\times10^{-3})$. Then the mass fraction of the neutron source has to be

$$X_{\rm ns}=AY_{\rm ns}\cong Af(1.92\times10^{-3}) . \quad (10)$$

From $\tau\cong0.05$ s and Eq. (8) follows the condition for the He abundance

$$\rho Y_\alpha\cong\frac{1}{0.05N_A\langle\sigma v\rangle_{(\alpha,n)}} . \quad (11)$$

Because the thermonuclear reaction rate for charged-particle induced reactions is temperature dependent, the latter expression cannot be simplified further. It should be noticed that Eq. (11) might be hard to fulfill. In a solar mix, with ^{22}Ne being the neutron source and an abundance equal to ^{14}N after all CNO nuclei were converted, one obtains $f\cong10$ (see, e.g., Figs. 1 and 2 in Thielemann *et al.* [52]). This was also verified in recalculations with updated reaction rates. Part of the reason for this large factor is that ^{25}Mg, resulting from the (α,n) reaction on ^{22}Ne, is a strong neutron poison. When using ^{18}O as a neutron source, $f\cong5$ a somewhat smaller factor is required in the case of ^{13}C ($f\cong3$). With these f values, Eq. (11) would require minimum mass fractions of 15% for ^{13}C, and as much as 40% for ^{22}Ne, the latter value certainly not being attained in astrophysically reasonable conditions. The results by Ziegert *et al.* [45] and Hillebrandt *et al.* [46] gave solutions in a pure mathematical sense for the free parameters of neutron density and exposure time. Whether they can be fulfilled seems to be marginal; a ^{13}C source would provide the best conditions. The half-life of ^{44}S ($T_{1/2}\cong310$ ms) was decisive for requiring an exposure time of $\tau\cong0.05$ s, which is hard to fulfill in He zones of massive stars during a supernova explosion. He-shell flashes in accreting white dwarfs and ^{13}C flashes in a yet undetermined site could perhaps fulfill this constraint (see, e.g., Hillebrandt *et al.* [57]). It is, however, important to test whether new experimental information on neutron-rich isotopes can change the previous constraints and whether the now also observed ^{58}Fe and ^{64}Ni enhancements can be attained as well.

D. Status after the present experiment

Major changes are the considerably shorter half-lives of ^{44}S (0.12 s compared to 0.31 s [16]) and ^{45}Cl (0.4 s compared to 1.7 s [17]), which is indicated in Fig. 10. At a first glance, this seems to strongly worsen the conditions. In order to get a similarly small leakage from S to Cl as discussed in Sec. V B, the process time would have to be shortened from 50 ms to $0.12/0.31\times50\cong20$ ms. This makes the astrophysical likeliness of such a process even smaller than with the previous 50 ms. On the other hand, the shorter half-life of ^{45}Cl allows a leakage of the Cl chain into the even-Z chain of Ar, where neutron capture cross sections are large and the mass $A=46$ is bypassed fast. Portions of the flow which stay in the Cl chain do not have such a negative effect, because of the smaller P_n value for the β decay of ^{47}Cl and the larger P_n value of ^{46}Cl, both less contributing to the final ^{46}Ca abundance. This behavior can already be recognized in Fig. 8 (although still calculated without making use of the new experimental information).

Only the curve with a neutron density of 5×10^{-5} mol cm^{-3} and an exposure time of 900 ms at the first peak results in time scales of the order of 1 s. There, the Y(^{48}Ca)/Y(^{46}Ca) ratio is rising again to a second peak for larger exposures $\rho Y_n\tau$ beyond 10^{-4} mol cm^{-3} s or $\tau\geq2$ s. This is due to the leakage from the Cl chain to Ar (which is still very small for the old ^{45}Cl half-life). With half-lives of 0.3 s for ^{44}S and 0.18 s for ^{46}Cl and a total neutron-capture time scale for $\rho Y_n=5\times10^{-5}$ mol/cm^3 and the reaction path in the S to Ar chains in Fig. 7 of

$$0.16\,\text{s}\ (^{40}\text{S})+0.076\,\text{s}\ (^{41}\text{S})+0.33\,\text{s}\ (^{42}\text{S})$$
$$+0.14\,\text{s}\ (^{43}\text{S})+0.007\,\text{s}\ (^{44}\text{Cl})+1.07\,\text{s}\ (^{45}\text{Cl})$$
$$+0.055\,\text{s}\ (^{46}\text{Ar})+0.14\,\text{s}\ (^{47}\text{Ar})=1.93\,\text{s} ,$$

the maximum abundance would occur in ^{48}Ar after $0.31[T_{1/2}(^{44}\text{S})]+0.18[T_{1/2}(^{45}\text{Cl})]+1.93=2.5$ s. After 2 s ($\rho Y_n\tau\geq10^{-4}$) we see already the rise to that peak. With the new ^{44}S and ^{45}Cl half-lives of 0.12 and 0.4 s we can

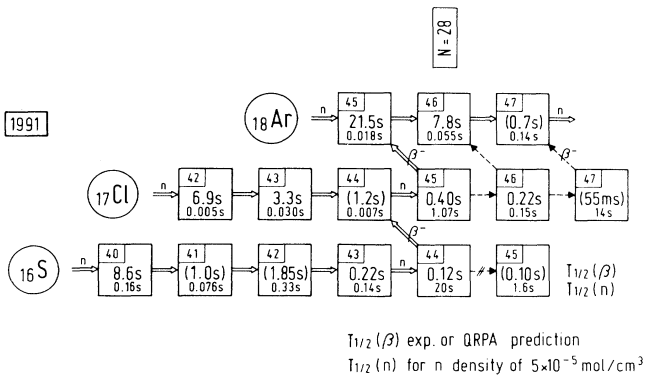

FIG. 10. Neutron capture path in the $_{16}$S to $_{18}$Ar chains [7] for a stellar temperature of $T=8\times10^8$ K and a neutron density of 5×10^{-5} mol cm^{-3} with our new experimental data. At both $N=28$ "turning-point" isotopes, ^{44}S and ^{45}Cl, β decay back to stability starts to dominate over further neutron capture. Hence, the possible $A=46$, 47 progenitors of ^{46}Ca will be produced in small amounts only. With this, large ^{48}Ca/^{46}Ca ratios can be obtained, as required to explain the observed abundances in EK-1-4-1. In the earlier approach of [46], neutron capture in the $_{17}$Cl chain proceeded up to ^{46,47}Cl which had put constraints on the P_n value of ^{47}Cl (for discussion, see text and Fig. 8).

reach the same situation via the reaction path of Fig. 10 already after 0.12 s+0.4 s+0.925 s=1.45 s or $\rho Y_n \tau = 7.25 \times 10^{-5}$ mol cm^{-3} s, and the rise of $Y(^{48}\text{Ca})/Y(^{46}\text{Ca})$ in Fig. 8 would start at $\rho Y_n \tau = 5 \times 10^{-5}$ mol cm^{-3} s. The required exposure time change by about a factor of 2, due to the changes in β-decay half-lives, would shrink the abscissa of the 5×10^{-5} curve in Fig. 8 by that factor, accordingly. Therefore, values of $\tau \cong 1.45$ s and $\rho Y_n \tau \cong 5 \times 10^{-5}$ mol cm^{-3} s would result in a maximum of the ^{48}Ca/^{46}Ca ratio. The larger branching into β decay at ^{45}Cl due to the half-life change by a factor of 4 would increase the 48/46 ratio in addition. These conclusions, coming from a first analytical analysis of the present experimental findings, change the constraints on exposure time from $\tau \cong 0.05$ s to $\tau \geq 1$ s, while leaving the total neutron exposure of about 5×10^{-5} mol cm^{-3} s practically unchanged.

E. Astrophysical sites

The exposure time scale $\tau \geq 1$ s, resulting from the above estimate, is now in accordance with any type-II supernova site. The neutron exposure $\rho Y_n \cong 5 \times 10^{-5}$ mol cm^{-3} results in a neutron number density of $n_n = \rho N_A Y_n \cong 3 \times 10^{19}$ cm^{-3}. This is a large neutron density, close to the smallest components in r-process conditions ($n_n > 10^{20}$ cm^{-3}, see Thielemann *et al.* [58] and Kratz *et al.* [59]) and hardly reachable in explosive He burning as already discussed in Sec. V C (see also [52,49,50]). A site adjacent to the r process, deep in the interior of a supernova core, but slightly further out in radius, where smaller neutron densities are expected, seems to be the most logical choice.

This is also the region of neutron-rich explosive Si burning and thus very similar to the scenario suggested by Hartmann *et al.* [44]. The main difference is that, in type-II supernovae, all of the explosive Si zones experience an *alpha-rich* freeze-out [60–62] (so called when, at high temperature, a large fraction of α particles formed during the NSE, is expanded and cooled so rapidly that not all the alphas have time to reassemble) and not a *normal* freeze-out as assumed in the MZM model. The final composition of the elements will then differ substantially. Hence, it seems that with a straightforward application, both of the initially suggested scenarios, our βn_d process and the multizone NSE approaches converge. They both have to be recalculated now, including the new experimental findings and a full treatment of the alpha-rich freeze-out. The alpha-rich freeze-out automatically provides large abundances of even-Z nuclei which act as seed for the βn_d version of a rapid neutron capture, in a similar way as the solar abundances used in our previous calculations.

The correlation with r-process enhancements in Sm, Nd, Ba [32,33], and Zr [40] underlines that the isotopic pattern in the Ca-Ti-Cr anomalies and the r-process contributions could come from the same astrophysical source. In general, we expect mixed compositions from supernovae. In the type-II supernova SN 1987A, mixing of the ejecta was evident from the widths of spectral lines in the infrared and the early emergence of x-rays and γ-rays, originating from the γ irradiation following the decay of ^{56}Ni and ^{56}Co (see, e.g., Arnett *et al.* [63]). Theoretical models of convective overturn and instabilities behind the propagating shock front also predict mixing of the ejecta [64–66], especially close to the neutron-star mass cut where r-process and neutron-rich Si burning are located.

VI. SUMMARY AND CONCLUSIONS

The half-lives and P_n values of ^{44}S and ^{45}Cl obtained in the present experiment deviate from straightforward shell-model predictions assuming spherical shapes for these semimagic ($N=28$) nuclei. This may indicate collectivity, providing first evidence for a rapid vanishing of the $N=28$ shell strength below ^{48}Ca.

There partly unexpected nuclear properties of ^{44}S and $^{45-47}$Cl give the clue to an understanding of isotopic anomalies in this region. With the new nuclear physics parameters, the problem of producing "very little" ^{46}Ca in a high-density βn_d process seems to be solved. But, in order to confirm the simultaneous production of "much" ^{48}Ca, the nuclear properties of $^{48-50}$Ar nuclei (as possible progenitors of ^{48}Ca) have to be determined experimentally.

In a broader context, the observed correlation of the Ca-Ti-Cr abundances with overabundances in ^{56}Fe, ^{64}Ni, ^{66}Zn (raising the question whether these elements are, indeed, produced in a single process) strengthens the necessity of studying nuclear properties of a hitherto virgin region of neutron-rich Sc to Mn isotopes. Information of the $T_{1/2}$ trends as a function of mass-number are required to reduce the uncertainties in the extrapolation to the turning points at the neutron-rich $A \cong 56$, 64, and 66 progenitors of the overabundant Fe-Ni-Zn nuclides. Finally, "complete" astrophysical network calculations with improved nuclear physics data are required, including a full treatment of the α-rich freeze-out both in the MZM model and in the βn_d process.

ACKNOWLEDGMENTS

We want to thank A. G. W. Cameron, C. Harper, D. Hartmann, and B. S. Meyer for stimulating astrophysical discussions. We also like to thank all the technical LISE/GANIL staff for their assistance during this experiment as well as the GANIL/JINR (Dubna) operating crew for delivering the ^{48}Ca beam. One of us (O.S.) would like to address special thanks to E. Kashy for his fruitful helps and discussions during the data analysis. This research was supported by NSF Grant No. AST-8913799, DFG (Kr806/1), BMFT (06MZ106).

[1] G. Münzenberg, Nucl. Phys. **A502**, 571c (1989).
[2] M. Weber, C. Donzaud, J. P. Dufour, H. Geissel, A. Grewe, D. Guillemaud-Mueller, H. Keller, M. Lewitowicz, A. Magel, A. C. Mueller, G. Münzenberg, F. Nickel, M. Pfützner, A. Piechaczek, M. Pravikoff, E. Roeckl, K. Rykaczewski, M. G. Saint-Laurent, I. Schall, C. Stéphan, K. Sümmerer, L. Tassan-Got, D. J. Vieira, and B. Voss, Z. Phys. A **343**, 67 (1992).
[3] M. Lewitowicz, R. Anne, A. G. Arthukh, D. Bazin, C. Borcea, V. Borrel, P. Bricault, C. Détraz, S. Dogny, D. Guillemaud-Mueller, J. C. Jacmart, C. Jonston, E. Kashy, H. V. Klapdor, S. M. Luckyanov, A. C. Mueller, Yu. E Penionzhkevich, F. Pougheon, A. Richard, M. G. Saint-Laurent, A. Staudt, and W. D. Schmidt-Ott, in *Proceedings of the 2nd International Conference on Radioactive Nuclear Beams,* Louvain-La-Neuve, Belgium, 1991, edited by T. Delbar (Bristol, 1992).
[4] D. Guillemaud-Mueller, C. Détraz, M. Langevin, F. Naulin, M. de Saint-Simon, C. Thibault, F. Touchard, and M. Epherre, Nucl. Phys. **A426**, 37 (1984).
[5] *Proceedings of the Workshop Nuclear Structure of Light Nuclei Far from Stability,* Experiment and Theory, Obernai, France, 1989, edited by G. Klotz (CRN, Strasbourg, 1991), see contributions by G. Walter (p. 85); A. Poves and J. Retamosa (p. 101); G. Audi (p. 113), K. Heyde (p. 129); B. A. Brown, E. K. Warburton, and B. H. Wildenthal (p. 147); R. J. Lombard (p. 299).
[6] N. Fukunishi and T. Otsuka, in *Proceedings of the International Symposium on Structure and Reactions of Unstable Nuclei,* Niigata, Japan, 1991, edited by K. Ikeda and Y. Suzuki (World Scientific, Singapore, 1992), p. 116.
[7] K-L. Kratz, R. Anne, D. Bazin, C. Borcea, V. Borrel, C. Détraz, S. Dogny, H. Gabelmann, D. Guillemaud-Mueller, W. Hillebrandt, M. Lewitowicz, S. M. Lukyanov, P. Moeller, A. C. Mueller, Yu. E. Penionzhkevich, B. Pfeiffer, F. Pougheon, M. G. Saint-Laurent, V. S. Salamatin, F. Schäfer, H. Sohn, O. Sorlin, F. K. Thielemann, and A. Wöhr, in *Proceedings of the 1st European Biennial Workshop on Nuclear Physics,* Mégève, France, 1991, edited by D. Guinet and J. P. Pizzi (World Scientific, Singapore, 1991), p. 218.
[8] D. Guillemaud-Mueller, Yu. E. Benionzhkevich, R. Anne, A. G. Artukh, D. Bazin, V. Borrel, C. Détraz, D. Guerreau, B. V. Gvozdev, J. C. Jacmart, D. X. Jiang, A. M. Kalinin, V. V. Kamanin, V. B. Kutner, M. Lewitowicz, S. M. Lukyanov, A. C. Mueller, Nguyen Hoai Chau, F. Pougheon, A. Richard, M. G. Saint-Laurent, and W. D. Schmidt-Ott, Z. Phys. A **332**, 189 (1989).
[9] S. M. Lukyanov, A. G. Artukh, B. A. Gvozdev, V. B. Kutner, Yu. E. Penionzhkevitch, L. Bex, M. P. Bourgarel, and J. Ferme, Nucl. Instrum. Methods B **47**, 102 (1990).
[10] R. Anne, D. Bazin, A. C. Mueller, J. C. Jacmart, and M. Langevin, Nucl. Instrum. Methods A **257**, 215 (1987).
[11] F. Hubert, R. Bimbot, and H. Gauvin, At. Data Nucl. Data Tables **46**, 1 (1990).
[12] A. C. Mueller, D. Bazin, W. D. Schmidt-Ott, R. Anne, D. Guerreau, D. Guillemaud-Mueller, M. G. Saint-Laurent, V. Borrel, J. C. Jacmart, F. Pougheon, and A. Richard, Z. Phys. A **330**, 63 (1988).
[13] J. P. Dufour, S. Beraud-Sudreau, R. Del Moral, H. Emmermann, A. Fleury, F. Hubert, C. Poirot, M. S. Pravikoff, J. Fréhaut, M. Beau, A. Bertin, G. Giraudet, A. Huck, G. Klotz, C. Miehé, C. Richard-Serre, and H. Delagrange, Z. Phys. A **319**, 237 (1984).
[14] F. James and M. Roos, CERN library, D506 MINUIT.
[15] H. Otto and W. Ziegert, Institut für Kerchemie library, Mainz, Germany.
[16] M. Lewitowicz, Yu. E. Penionzhkevich, A. G. Artukh, A. M. Kalinin, V. V. Kamanin, S. M. Lukyanov, Nguyen Hoai Chau, A. C. Mueller, D. Guillemaud-Mueller, R. Anne, D. Bazin, C. Détraz, D. Guerreau, M. G. Saint-Laurent, V. Borrel, J. C. Jacmart, F. Pougheon, A. Richard, and W. D. Schmidt-Ott, Nucl. Phys. **A496**, 477 (1989).
[17] H. V. Klapdor, J. Metzinger, and T. Oda, At. Nucl. Data Tables **31**, 81 (1984).
[18] J. Krumlinde and P. Möller, Nucl. Phys. **A417**, 419 (1984).
[19] A. Staudt, E. Bender, K. Muto, and H. V. Klapdor, At. Data Nucl. Data Tables **44**, 1 (1990).
[20] P. Möller and J. Randrup, Nucl. Phys. **A541**, 1 (1990).
[21] P. Möller and J. R. Nix, At. Data Tables **39**, 213 (1988).
[22] P. Möller, W. D. Myers, W. J. Swiatecki, and J. Treiner, At. Data Nucl. Data Tables **39**, 225 (1988); and private communication (1992).
[23] P. Möller and J. R. Nix, Proceedings of the 6th Conference on Nuclei Far from Stability, Bernkastel-Kues, Germany, 1992, in press.
[24] J. M. Pearson, Y. A. Aboussir, A. K. Dutta, R. C. Navak, M. Farine, and F. Tondeur, Nucl. Phys. **A528**, 1 (1991); and private communication (1992).
[25] K.-L. Kratz, Rev. Mod. Astron. **1**, 184 (1988).
[26] G. Audi and A. H. Wapstra, private communication (1992).
[27] I. Ragnarsson and R. K. Sheline, Phys. Scr. **29**, 385 (1984).
[28] K.-L. Kratz, B. Pfeiffer, A. Wöhr, and P. Möller, Z. Phys. A **332**, 419 (1989).
[29] P. Möller and J. R. Nix, Nucl. Phys. **A536**, 20 (1992).
[30] A. C. Mueller and R. Anne, Nucl. Instrum. Methods **B56/67**, 559 (1991).
[31] T. Lee, D. A. Papanastassiou, and G. J. Wasserburg, Astrophys. J. Lett. **220**, L21 (1978).
[32] M. T. McCulloch and G. J. Wasserburg, Astrophys. J. Lett. **220**, L15 (1978); Geophys. Res. Lett. **5**, 599 (1978).
[33] G. W. Lugmair, K. Marti, and N. B. Scheinin, Lunar Planet. Sci. **IX**, 672 (1978).
[34] F. R. Niederer, D. A. Papanastassiou, and G. J. Wasserburg, Geochim. Cosmochim. Acta **45**, 1017 (1981).
[35] J.-L. Birck and C. J. Allegre, Geophys. Res. Lett. **11**, 943 (1984).
[36] J.-L. Birck and G. W. Lugmair, Earth Planet Sci. Lett. **90**, 131 (1988).
[37] D. A. Papanastassiou and C. A. Brigham, Astrophys. J. Lett. **338**, L37 (1989).
[38] J. Völkening and D. A. Papanastassiou, Astrophys. J. Lett. **347**, L43 (1989).
[39] R. D. Loss and G. W. Lugmair, Astrophys. J. Lett. **360**, L59 (1990).
[40] C. L. Harper, L. H. Nyquist, C.-Y. Shih, and H. Wiesmann, in *Nuclei in the Cosmos,* Proceedings of the first International Symposium on Nuclear Astrophysics, Baden/Vienna, 1990, edited by H. Oberhummer and W. Hillebrandt (MPI für Physik und Astrophysik, Garching), MPA/P4, p. 138.
[41] A. G. W. Cameron, Astrophys. J. Lett. **230**, L53 (1979).
[42] D. G. Sandler, S. E. Koonin, and W. A. Fowler, Astrophys. J. **259**, 908 (1982).
[43] M. Harris, Astrophys. J. **264**, 613 (1983).
[44] D. Hartmann, S. E. Woosley, and M. F. El Eid, Astro-

phys. J. **297**, 837 (1985).
[45] W. Ziegert, M. Wiescher, K.-L. Kratz, P. Möller, J. Krumlinde, F.-K. Thielemann, and W. Hillebrandt, Phys. Rev. Lett. **55**, 1935 (1985).
[46] W. Hillebrandt, K.-L. Kratz, F.-K. Thielemann, and W. Ziegert, in *Weak and Electromagnetic Interactions in Nuclei,* edited by H. V. Klapdor (Springer-Verlag, Berlin, 1986), p. 987.
[47] T. Lee, in *Meteorites and the Early Solar System,* edited by J. F. Kerridge and M. S. Mathews (University of Arizona Press, Tucson, 1988), p. 1063.
[48] K.-L. Kratz, W. Ziegert, W. Hillebrandt, and F.-K. Thielemann, Astron. Astrophys. **125**, 381 (1983).
[49] J. B. Blake, S. E. Woosley, T. A. Weaver, and D. N. Schramm, Astrophys. J. **248**, 315 (1981).
[50] J. J. Cowan, A. G. W. Cameron, and J. W. Truran, Astrophys. J. **294**, 656 (1985).
[51] J. W. Truran, J. J. Cowan, and A. G. W. Cameron, Astrophys. J. Lett. **222**, L63 (1978).
[52] F.-K. Thielemann, M. Arnould, and W. Hillebrandt, Astron. Astrophys. **74**, 175 (1979).
[53] W. Ziegert, Thesis, *Universität Mainz, 1985.*
[54] A. G. W. Cameron, in *Essays in Nuclear Astrophysics,* edited by C. A. Barnes *et al.* (Cambridge University Press, 1982), p. 23.
[55] Z. Y. Bao and F. Käppeler, At. Nucl. Data Tables **36**, 411 (1987).
[56] E. Anders and N. Grevesse, Geochim. Cosmochim. Acta **53**, 197 (1989).
[57] W. Hillebrandt, W. Ziegert, F.-K. Thielemann, and K. Nomoto, in *Advances in Nuclear Astrophysics,* edited by E. Vangioni-Flam *et al.* (Editions Frontières, Gif-sur-Yvette, 1987), p. 233.
[58] F.-K. Thielemann, J.-P. Bitouzet, K.-L. Kratz, P. Möller, J. J. Cowan, and J. W. Truran, Phys. Rep. (to be published).
[59] K.-L. Kratz, J.-P. Bitouzet, F.-K. Thielemann, P. Möller, and B. Pfeiffer, Astrophys. J. **403**, 216 (1993).
[60] F.-K. Thielemann, M. Hashimoto, and K. Nomoto, Astrophys. J. **349**, 222 (1990).
[61] S. E. Woosley and R. Hoffman, Astrophys. J. **395**, 202 (1992).
[62] B. S. Meyer, G. J. Mathews, W. M. Howard, S. E. Woosley, and R. D. Hoffman, Astrophys. J. **399**, 656 (1992).
[63] W. D. Arnett, J. N. Kirshner, and S. E. Woosley, Annu. Rev. Astron. Astrophys. **27**, 629 (1989).
[64] W. D. Arnett, B. Fryxell, and E. Müller, Astrophys. J. Lett. **341**, L63 (1989).
[65] M. Herant and W. Benz, Astrophys. J. Lett. **370**, L81 (1991).
[66] M. Herant, W. Benz, and S. Colgate, Astrophys. J. **395**, 642 (1992).